Electrical and Spectroscopic Characterization of Metal/Monolayer/Si Devices

Curt A. Richter,*,† Christina A. Hacker,† and Lee J. Richter‡

Semiconductor Electronics Division and Surface and Microanalysis Science Division, National Institute of Standards and Technology, 100 Bureau Drive, Gaithersburg, Maryland 20899

Received: June 29, 2005; In Final Form: September 23, 2005

A simple technique for vibrational spectroscopy of metal/monolayer/silicon structures is applied to study the interaction of Au, Al, and Ti with alkane monolayers, either assembled onto thin oxides or directly attached to Si. The results are correlated with current−voltage and capacitance−voltage measurements. Alkane films on oxides are found to be robust with respect to the deposition of Au and Al and are partially consumed during the deposition of Ti. In contrast, alkoxy films directly attached to H-terminated Si via an ether linkage are displaced by all three metals. The vibrational data are positively correlated with the electrical data to establish an improved understanding of the interactions at the buried metal/monolayer interface. The results demonstrate extreme sensitivity of the monolayer/metal reactivity to the nature of the film/substrate bonding.

Introduction

The buried interface between metals and thin organic films is critical to a diversity of technologies, from bonding/adhesion to corrosion resistance. Because of the ability to prepare well-defined organic surfaces, the interface between metals and self-assembled monolayer (SAM) films has been extensively studied as a model for more complex interfaces.[1] In recent years, the metal/monolayer/substrate system has become of considerable interest in its own right, due to wide interest in molecular electronics and other technological opportunities in the area of electronics. SAMs hold promise as replacement diffusion barriers and dielectrics in conventional semiconductor device architectures[2] and are being explored as active components in molecular electronic schemes.[3] Critical to the development of this last application is the correlation of electrical performance with molecular structure. A diversity of electrical behavior has been reported for molecular devices. In some, it is clear that the behavior is molecule independent; i.e., it is associated with the molecule−electrode combination in the measurement platform.[4,5]

The buried metal/monolayer/substrate interface is remarkably difficult to characterize in situ. Metal films become opaque to both optical and charge particle probes at thicknesses on the order of 10 nm. Therefore, the bulk of the analysis of metal/monolayer systems has been done either via the use of semitransparent metal layers or via destructive analysis. In the case of films on Si (an infrared (IR) transparent material) internal reflection techniques, both multiple[6] and grazing incidence[7] can be used. In this report, we present the results of a straightforward optical measurement, p-polarized backside reflection absorption infrared spectroscopy (pb-RAIRS). It is applicable to any metal/molecule/substrate system where the substrate is IR transparent. It has the advantage over internal reflection that special substrate shapes are not required; therefore, it can be extended to the direct study of patterned capacitors with the use of high brightness sources and grazing incidence microscopy. In addition, the accessible frequency range is not restricted by multiphonon absorption as in a multiple internal reflection geometry. However, the intrinsic sensitivity is less than the internal approaches. We apply pb-RAIRS to the characterization of the interface between vapor-deposited top metal contacts (Al, Au, and Ti with a Au overlayer) and alkane dielectric films attached to Si substrates. To determine the effect of monolayer structure, as determined by pb-RAIRS, on the end performance of molecular electronic devices, the results are directly correlated with electrical characterization of capacitor structures on identically fabricated films. The agreement of the results from these very different characterization approaches increases our confidence in both the experimental results and our interpretations. We find strikingly different behavior for films attached to thin oxides via hydrosilation reactions and films directly attached to Si via UV mediation. This variability in monolayer/top-metal reactivity for identical alkane surface functionality demonstrates the extreme importance of the film/substrate bonding and has ramifications on the design and fabrication of hybrid Si molecule electronic devices.

Experimental Section

Alkane monolayers from the reaction of octadecanetrichlorosilane (OTS) were formed on both thermal oxide and native oxide films. The substrates were double side polished Si(111) wafers (P doped, 8−12 Ω·cm). The wafers were first RCA cleaned. The resultant chemical oxide was stripped by buffered oxide etch prior to growth of the dry thermal oxide (800 °C with a 30-min densification anneal in N_2 at 1000 °C, 3.6 nm thick). For the native oxide samples (1.7 nm thick), the RCA oxide was strengthened by a 30-min treatment in a commercial UV−ozone cleaner (UVO). OTS was deposited by immersion of the substrates in a 2 mmol/L solution in hexadecane for 18 h. Immediately prior to immersion, both thermal and native oxide samples were cleaned by using a 5-min UVO treatment per side. All OTS processing was done in a class 10 000 clean room at a relative humidity of 45%. Upon removal from solution, the samples were cleaned by ultrasonic treatment in chloroform, isopropyl alcohol, and 18 MΩ·cm water and then annealed at 150 °C for 10 min. Thickness of the films was

* To whom correspondence should be addressed. E-mail: curt.richter@nist.gov.
† Semiconductor Electronics Division.
‡ Surface Microanalysis Science Division.

10.1021/jp053561r
Published on Web 11/02/2005

determined by spectroscopic ellipsometry (1.2−6.5 eV). The oxide thickness was determined from freshly UVO cleaned reference films by using a three-phase model (air, SiO_2, Si) and the SiO_2 index of refraction reported by Brixner.[8] The OTS film thickness was determined from a four-phase model (air, OTS, SiO_2, Si), fixing the oxide thickness at the reference film value and assuming an index of 1.5 for the OTS layer. The alkane film thickness on the native oxide samples was 2.6 ± 0.1 nm, while that on the thermal oxide was consistently lower: 2.3 ± 0.1 nm. We attribute the difference in the derived thicknesses of the OTS on the native and thermal oxides to the formation of slightly denser OTS films on the native oxides. Sessile drop water contact angles were 109 ± 1° and 106 ± 1° on the native and thermal oxide samples, respectively. Slightly denser films (2.9 ± 0.4 nm) were formed after air plasma treating the surfaces (2 min); however, the plasma treatment produced excessive charged defects at the interface, resulting in highly nonideal capacitors (see Supplemental Information). Alkoxy monolayers directly attached to Si were formed by the UV promotion of the reaction of dilute solutions of octadecyl alcohol (OA) in CH_2Cl_2 with the H-terminated Si(111) surface (H−Si) as described previously.[9,10] The resultant films are dense and covalently bonded to the Si(111) substrate. Direct attachment was indicated by the elimination of the Si−H vibrational features. The films were moderately robust to oxidative attack, as no Si−O−Si features were observed during brief (24 h) exposure to air. The ellipsometric thickness of the films was 2.2 ± 0.1 nm,[11] with typical water contact angles of 112°. The ellipsometric thickness indicates a slightly lower density for the directly attached films, compared to silanization, which has been attributed to packing constraints imposed by the Si lattice.[10]

Three top metal layers were deposited from physical evaporation sources: 200 nm of Al, 200 nm of Au, and 9 nm of Ti followed by 200 nm Au (Ti:Au).[12,13] The deposition rate was nominally 0.1 nm/sec for the first ∼10 nm and then (0.5−0.8) nm/sec for the remaining deposition. The evaporator base pressure prior to evaporation was 1.3 × 10^{-4} Pa (10^{-6} Torr) and did not exceed 1.3 × 10^{-3} Pa (10^{-5} Torr) during evaporation. The sources were ∼60 cm from the target. Blanket metal films were deposited on ∼(15 mm × 15 mm) samples for Fourier transform infrared (FTIR) characterization, while arrays of 150 μm diameter dots were deposited via a shadow mask to form simple capacitor structures for electrical characterization. The relatively large device area, the lack of a backside metal contact, and the dense spacing of the top-metal dots make these simple structures ideal for direct comparison with the pb-RAIRS measurements; however, these same features make these less than optimal electrical test structures.

Reference samples were created by deposition of the metals directly on the thermal and native oxide films, and on H−Si. The alkane films and metal depositions were performed via batch processing, providing a high degree of reproducibility. All IR spectra were recorded with a commercial Fourier transform instrument with a MCT detector at 8-cm^{-1} resolution. Scans (512) were co-added for a total data acquisition time of ∼6.5 min. p-Polarized Brewster-angle (∼73.7°) transmission spectra were acquired with a custom-built sample holder. p-Polarized, near-Brewster-angle, backside reflection spectra were acquired with a commercial 80° reflection accessory. The actual reflection angle was determined to be ∼76.5°. For both measurements, wire grid polarizers (on either ZnSe or BaF_2 substrates) were used to define the polarization. Figure 1 presents schematic diagrams for both the transmission and pb-RAIRS experimental configurations. All electrical measurements were performed with a commercial low-electronic noise probe station.

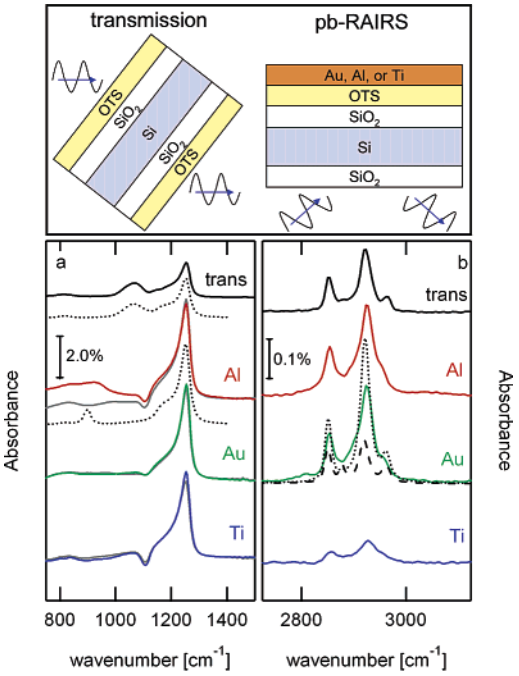

Figure 1. p-Polarized transmission and reflection IR spectra for OTS films assembled on thermal oxides. Black lines, p-Polarized transmission; color lines, metal/OTS/oxide; grey lines in (a) metal/oxide; Model spectra with isotropic (dotted lines) and biaxial (dashedlines) dielectric functions. Schematic: experimental configurations for (left) p-polarized Brewster-angle transmission and (right) pb-RAIRS. The film thicknesses are not draw to scale.

Results and Discussion

Siloxane Films. p-Polarized Brewster-angle transmission spectra of the double side functionalized alkane reference films on the thermal oxides (OTS/Thr) are shown in Figure 1. The spectra are referenced to a freshly prepared H−Si sample and agree with previous reports.[7,14] The dominant features in the oxide region are the Si−O−Si symmetric stretch (ν_{sym}) at ∼816 cm^{-1}, the Si−O−Si asymmetric TO phonon at 1066 cm^{-1}, and LO phonon at 1262 cm^{-1}. The negative dip at 1107 cm^{-1} is an artifact due to a slight miscancellation of the Si−O−Si stretch of bulk O impurities.[15] The dominant features in the C−H stretch region are the methylene symmetric stretch (d+ near 2850 cm^{-1}) and asymmetric stretch (d− near 2920 cm^{-1}). These stretch frequencies can be used to characterize the degree of order of the alkane backbone.[16,17] The observed C−H frequencies for OTS/Thr (Table 1) are consistent with a nearly all-trans, crystalline film. The observed C−H frequencies for the OTS on native oxide films (OTS/Nat, Table 1, spectra not shown) were consistently red shifted with respect to OTS/Thr, suggesting slightly better ordered, more dense films were formed on the native oxide, consistent with ellipsometry and contact angle.

Also shown in Figure 1 are the pb-RAIRS of the metalized films. The spectra are referenced to the appropriate metal deposited on an H−Si sample. It is essential that the entrance faces of the sample and reference be vibrationally equivalent. For the Au and Ti:Au samples, this was achieved by the following post metal deposition processing: 5-min UVO clean, 18-MΩ·cm water rinse, 3-min UVO clean, 18-MΩ·cm water rinse, HF strip, and 30-min UVO oxide growth. For the Al/OTS samples, it was found that the Al film delaminated upon contact with water. Therefore the Al/OTS samples were not

TABLE 1: Characteristic Vibrational Frequencies (cm^{-1})

	transmission			Al		Au		Ti:Au	
mode[a]	OTS/Nat	OTS/Thr	OA	OTS/Nat	OTS/Thr	OTS/Nat	OTS/Thr	OTS/Nat	OTS/Thr
d+	2851	2852	2855	2853	2854	2852	2853	2853	2855
r+	2879	2879	2880	NR[b]	NR	2873	NR	2870	2870
d−	2919	2921	2925	2923	2925	2923	2925	2925	2927
r−	2964	2964	2963	2960	2955	2958	2957	2956	2956

[a] Mode notation is that of ref 17. [b] Not resolved.

postmetalization processed. The vibrational contribution from the alkane film on the entrance face was subtracted based on detailed modeling and the transmission reference film (see Supplemental Information). In the low wavenumber region (800−1400) cm^{-1}, the spectrum is dominated by the Si−O LO phonon. A weak feature attributed to aluminum oxide is observed at ∼930 cm^{-1} for the Al/OTS/Thr and Nat samples. No alumina features were observed for Al/SiO_2, consistent with earlier work.[7] (The Si−O−Al vibration cannot be isolated from the Si−O symmetric stretch at 816 cm^{-1}.) No additional oxide features were observed for either the Au or Ti:Au films. Under the metal deposition conditions used in fabricating the samples, it is likely that oxides of Al and Ti will form,[18] and metal oxide control samples were fabricated to investigate the vibrational spectra that would be associated with possible metal oxides. Thin (∼2 nm) films of Ti and Al were oxidized by exposure to ambient atmosphere. Thick Au films were then deposited to form an IR-reflective top-metal to enable pb-RAIRS measurements. While a well-resolved AlO_x peak was observed at ∼930 cm^{-1} in the Al oxide control, no oxide peaks are clearly resolved in the Ti oxide sample.[19] For a thin TiO_2 film on a reflective substrate, the LO phonon appears as a broad feature[20] near 850 cm^{-1}. Our sensitivity to TiO_2 is poor, as the feature is nominally degenerate with the Si−O symmetric stretch at 813 cm^{-1}.

In the C−H stretch region, the vibrational spectra of the Al and Au metalized OTS films are very similar. The d− frequency shifts slightly to higher wavenumbers upon metal deposition, indicative of slight disordering of the chains due to weak interactions with the metal. Additionally, a new, broad, weak feature appears at ∼2825 cm^{-1}. This is attributed to a "soft" methylene mode,[21] indicating interaction of the methylenes with the deposited metal, suggestive of some degree of penetration of the film by the metal. The integrated intensity of the soft mode is 0.2 that of the d+ mode at 2853 cm^{-1}. In contrast to the Al and Au results, the Ti:Au metallization causes significant changes in the vibrational spectra. The intensities of all bands are severely reduced indicative of the partial consumption of the alkane monolayer, and the d− frequency appears at 2926 cm^{-1}, characteristic of a disordered liquid. The severe attenuation and disruption of the film is consistent with earlier studies of Ti on alkanes[6,22,23] and suggests chemical interaction between the Ti and the hydrocarbon, probably due to Ti carbide formation.[22]

We have attempted to gain further insights into the degree of interaction between the metal and the film by quantitative modeling of the FTIR spectra. This is essential, as the presence of the metal overlayer significantly changes the nature of the measurement. Shown in Figure 1a is a fit of the low wavenumber transmission spectrum to a five-phase model (air, oxide, silicon, oxide, air) where the silicon oxide is assumed to be 3.5-nm thick and has an isotropic dielectric function given by a constant and the sum of 3 Gauss−Lorentz vibrational features at 813, 1062, and 1188 cm^{-1}. These frequencies agree well with earlier studies of amorphous SiO_2.[7] Also shown in Figure 1a is forward simulated pb-RAIRS for the six-phase model: air, silicon, oxide, OTS (2.6 nm), amorphous alumina, Al.[24] The a-alumina film was assumed to be 0.1 nm thick. All other parameters of the reflection spectrum were fixed. The Si−O ν_{sym} and TO phonon are suppressed in the reflection spectrum compared to the transmission spectrum. This is because the presence of the metal over layer imposes the surface selection rule, and the reflection spectrum is dominated by the normal element of the film dielectric tensor, while the transmission spectrum, due to refraction, samples a nearly equal mix of the in-plane and normal components. There is a frequency shift between the alumina feature and that predicted by the literature dielectric function for a-alumina.[25] However, the comparison establishes that the alumina layer is of order ∼0.1 nm thick.

OTS functionalization is known to produce dense, well-ordered films with all-trans chains oriented near the surface normal.[26] This results in a highly birefringent (uniaxial) dielectric function ϵ for the alkane layer. We have developed a uniaxial model for the OTS films, based on fitting the p- and s-polarized Brewster-angle transmission spectra (see Supplemental Information for details).[14] Shown in Figure 1b as a dashed line is the expected reflection spectra if there is no perturbation of the film by the metal. Note that the unperturbed model does not well represent the observations. We have also simulated the reflection spectra, assuming the film has an isotropic dielectric function given by the average of the uniaxial film $\epsilon_{iso} = (2\epsilon_{||} + \epsilon_z)/3$. This is shown as the dotted line. This simulated spectrum does not include the line-broadening and frequency shifts arising from disorder in the film. However, the integrated intensity of the isotropic model is in fair agreement with the observed spectra, suggesting minimal loss of material from the organic film.

The direct current (dc) current−voltage (I−V) characteristics of the vertical capacitor device structures are shown in Figure 2. Simple tunneling theory cannot be used to analyze the IV

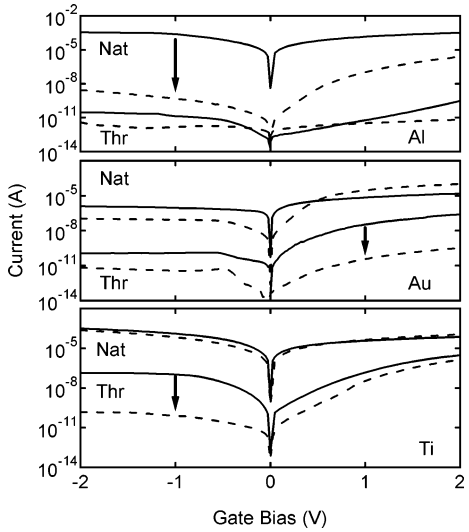

Figure 2. I−V characteristics for capacitors formed from the various metals on thin oxides and molecular films. Key: solid lines, metal/oxide; dashed lines, metal/molecule/oxide.

curves because the thin oxide and monolayers do not form ideal tunnel barriers. Also, simple metal/semiconductor contact (Schottky) theory does not completely describe the IV data because the top metallization does not form clean metal/semiconductor−substrate contacts through the thin oxides and monolayers. Because a quantitative description of these IV curves is challenging, we have taken a qualitative approach to analysis of the IV data. The native oxide is a poor dielectric, and the metals deposited on the native oxide reference films exhibit behavior qualitatively expected for metal/semiconductor junctions. Au is most strongly rectifying (on these n-type Si substrates) due to its large work function. Because of the light substrate doping and lack of a backside metal contact necessary for IR transmission, electrical substrate contact is not optimal, and there is some unavoidable sample-to-sample variability.[27] The presence of the OTS film significantly decreases the amplitude of the leakage current for the case of Al and Au, indicating (1) the presence of an OTS/oxide dielectric stack and (2) that there is minimal metal penetration of the OTS film. The Ti:Au metalization results in intermediate current blocking behavior: the OTS functionalization still seems to prevent metal penetration of the OTS; however, the dielectric stack resistance is low, which is suggestive of a relatively thinner OTS/oxide dielectric stack. The reference capacitors on the thermal oxides behave more ideally. Even with this thicker, higher-quality SiO_2, there is marked improvement in the blocking characteristics of the dielectric with the addition of the OTS films.

A simple estimate of the upper limit on the area of metal interpenetration can be determined (from comparison of the OTS/oxide and oxide-control IV data) by assuming the OTS areas are fully blocking and attributing all current to fully penetrating metal asperities. The $\sim 10^6$ decrease in current at 1 V for the Al/OTS/Nat device implies a defect density $\leq 10^{10}$ cm^{-2}. FTIR can also determine an upper limit by using an effective medium model for the mixed metal/molecule layer similar to that used by Beirhals et al.[7] to estimate the density of Al asperities in thermally stressed $Al/SiO_2/Si$ capacitors. FTIR places an upper limit of ∼1% metal fraction in the layer. These estimates demonstrate that electrical measurements are much more sensitive to defects than the FTIR.

To characterize the metal molecule interactions further, alternating current (ac) capacitance−voltage (CV) curves were taken on 150-μm diameter dot capacitors identical to those used for the IV measurements for all the combinations of top-gate metals (Au, Al, and Ti) and dielectric/substrates (OTS/Thr, Thr, OTS/Nat, Nat, C18O, and H-terminated). Figure 3 compares typical results for CV measurements of metal/OTS/Thr devices and metal/Thr control samples for all three metals. In each case, the accumulation capacitance value (observed for positive biases) is decreased by the OTS monolayer. This change in the accumulation capacitance value indicates that in all cases the OTS monolayer is behaving as a dielectric layer; i.e., the total effective thickness of the OTS/Thr dielectric stack is thicker than the total effective thickness of the thermal oxide layer alone. Easily analyzed data could not be obtained from capacitor devices formed directly on the native oxide due to the large dc leakage currents. Typically, acceptable CV curves were measured for the metal/OTS/Nat samples, confirming that the OTS monolayers are blocking current and leading to effectively thicker dielectric stacks than native oxide alone.

By presumption of two capacitors in series, (C_{SiO2} and C_{alkane}), the dielectric thickness of the alkane films can be extracted from the CV characteristics of the OTS/Thr devices by using the values for C_{SiO2} experimentally measured for the thermal oxide control samples and based on a dielectric constant of 2.5 (at 1 kHz) for the alkane monolayer. For the Ti/OTS devices, an OTS thickness of 0.7 nm was extracted. This is consistent with the pb-RAIRS (integrated intensity of the d+ and d− bands was 0.2 that of the isotropic reference spectrum implying ∼0.5 nm of remaining hydrocarbon) and supports the hypothesis of film consumption due to carbide formation. For the Al and Au devices, an OTS electrical thickness of 1.5 nm was determined. In the pb-RAIRS, the integrated d+ and d− intensities of the main features was ∼0.7 that of the isotropic reference (implying a thickness ∼1.8 nm), while the ratio of the soft d+ (2825 cm^{-1}) to the main d+ (2852 cm^{-1}) was 0.2. The electrical and optical data are most consistent with a thin (∼0.5 nm) selvage region characterized by partial metal penetration into the film.

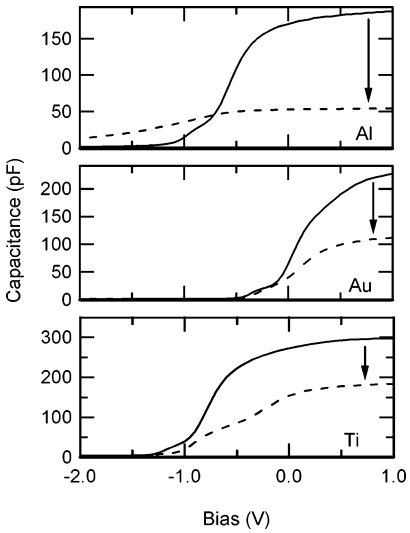

Figure 3. Capacitance−voltage curves. Top: Al top metal on ∼3.5-nm thermally grown SiO_2 [Thr] (solid line) and Al metal on OTS/Thr stack (dashed line). Middle: Au on ∼3.5-nm Thr (solid line) and Au on OTS/Thr stack (dashed line). Bottom: Ti on ∼3.5-nm Thr (solid line) and Ti on OTS/Thr stack (dashed line). All CV curves shown are obtained at 1 kHz.

The deposition of Al, Au, and Ti has been extensively studied on self-assembled monolayers of functionalized alkane thiols on Au substrates. The deposition of Au on aliphatic films results in extensive penetration of the film by the Au (attributed to a dynamic defect mechanism mediated by the low corrugation for thiol linkages to Au), and the molecular film "floats" on the deposited metal.[28] For Al, the first monolayer of metal penetrates and forms a Au−Al alloy.[29] However, the subsequent metal forms a layer on top of the alkane film, presumably due to higher corrugation for the thiol−Al linkage. For Ti, extensive reaction with the film is observed.[6,22,23] Our spectroscopic results are consistent with this earlier work and the assumption that the dynamic defect mechanism is shut down by the rigid siloxane linkage of the alkane film. While it is clear that both Al and Au perturb the nearly ideal ordering of the chains, we do not observe as great a metal−molecule interaction as reported by Jun et al. on Au/OTS/Si via ATR.[6] In our study, the full width at half maximum of the d− broadens from 20 ± 1 cm^{-1} for the as-assembled films to 24 ± 1 cm^{-1} for both Au and Al, compared to 46 cm^{-1} in ref 6. The origin of this discrepancy is unclear.

Directly Attached Alkoxy Films. Shown in Figure 4a is the p-polarized Brewster-angle transmission IR spectrum for a C18 alkoxy film directly attached to Si via UV-assisted addition of octadecyl alcohol to H-terminated Si(111). Also shown in Figure 4 are the pb-RAIRS spectra following the deposition of Al, Au,

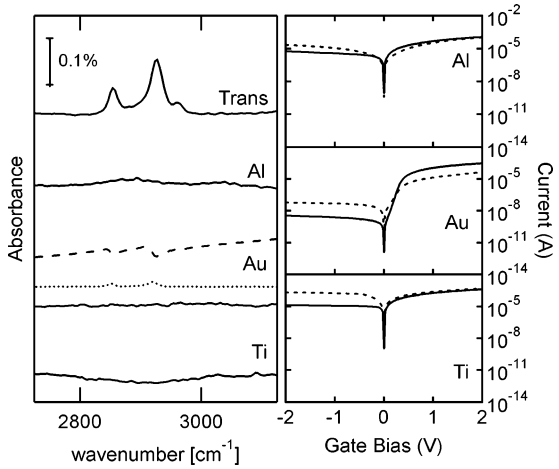

Figure 4. p-RAIRS and IV measurements for octadecyl alcohol films directly attached to silicon. (left) p-Polarized transmission and reflection IR spectra (solid lines). Broken lines are EMA-generated model spectra: Bruggeman (dotted); Looyenya (dashed). (right) I−V characteristics of capacitors formed from the various metals on H−Si (solid) and OA−Si (dashed).

and Ti. In all three cases, there are no detectable hydrocarbon features in the spectra. Simulated spectra based on either a Bruggeman or Looyenya effective medium approximation for a molecular film with 50% metal fraction are shown in Figure 4a. Weak CH features are still present. These simulations strongly suggest that the metals have displaced the alkoxy films, severing the C−O−Si covalent linkage.

The displacement of the molecular film is consistent with the I−V characteristics shown in Figure 4b. Reference devices, formed by direct deposition of the respective metal on the H-terminated surface, exhibit the expected metal/semiconductor behavior with Au on n-Si devices once again most rectifying. The changes in the I−V characteristics upon introduction of the directly attached alkoxy film are very different than in the case of OTS/oxide. There is no evidence of significant blocking behavior due to the presence of the alkoxy molecular film. In fact, for Al and Ti, there is an *increase* in the reverse bias leakage, while for Au, there is a slight decrease in the rectification and a decrease in the forward bias current. We propose that the process by which the metal displaces the molecular film creates a metal/semiconductor interface that is less ideal than when the top metal is directly deposited on pristine H-terminated Si surfaces. This causes a lowering of the Schottky barrier (with respect to that at the ideal metal/H−Si interface) that leads to the observed IV curves having a greater reverse current leakage. C−V measurements (not shown) are also consistent with a direct metal/Si interface.

The displacement of the directly attached films is remarkable, in light of the robust behavior of the silane-derived films. The displacement of the films cannot be attributed solely to film quality, as we have formed poor siloxane derived films (ellipsometric thickness, 1.8 nm; d−, 2925 cm^{-1}) and observed IR and I−V characteristics similar to those reported in Figures 1 and 2. The current results imply that the reactivity of alkoxy monolayers with metallization is intrinsically different than siloxane films. Since this difference in reactivity does not arise from differences in the monolayer structure, the likely source is the substrate−molecule interfacial chemistry. Both monolayers are expected to form strong covalent bonds with the OTS linked through a $C-Si(OSi)_3$ and the octadecyl alcohol linked through a $C-O-Si(Si)_3$ bond. The reported bond strengths for Si−O and Si−C linkages are nearly equivalent (Si−C, 369 kJ/mol; Si−O, 368 kJ/mol).[30] While alcohol derived films are moderately stable in air, and aldehyde derived films are stable for 30 min in 60 °C water,[10] previous reports of C−O−Si linkages have observed alkoxy monolayers are less stable toward oxidation than R−Si films.[31] The instability of the C−O−Si can be understood from organosilicon chemistry where it is known that the Si−O bond is slightly polar due to electronegativity differences, which in turn activates adjacent bonds in the molecules toward hydrolysis, reaction with fluoride ions, and heterolytic fission reactions.[32] Thus, it seems likely the alcohol films were displaced upon metallization due to severing the Si−Si back bonds. In fact, it has been reported that the reaction of ethanol with porous silicon results in etching of the Si via cleavage of the Si−Si back bonds.[33] However, reactions of alcohols do not etch single-crystal silicon and result in the formation of R−O−Si monolayers on the intact single-crystal surface.[10,34] Further work is under way to understand the detailed nature of the metal/monolayer/substrate reactions. While previous studies have determined differing headgroups have dramatic implications for the monolayer stability after metallization,[35] our work illustrates that the substrate−monolayer interfacial chemistry also plays a key role in the reactivity of organic monolayers with metallization.

It is interesting to note that, even in the case of the highly reactive Ti, the entire alkoxy film is displaced from the interface. This implies that the Ti does not uniformly attack the film and thus form a passivating TiC selvedge region as seen for the OTS films. Instead, the Ti migrates to the interface, presumably due to static defects within the organic layer, and attacks the $C-O-Si-Si_{bulk}$ linkage, "unzipping" the monolayer. This is consistent with recent detailed studies of Ti on methoxy terminated thiol SAMs on Au, in which chemical degredation of the films was found to be spatially heterogeneous.[36]

Very little electrical characterization has been performed on directly attached films. In an earlier report, NIST-presented C−V characterization of vapor deposited Al top contact, octadecyl alcohol derived films.[9] The observed yield for blocking devices was extremely low. This is consistent with displacement of the molecules in the majority of the devices. C−V measurements have also been reported for vapor-deposited Al on octadecene derived films[37] and for Hg drop electrodes on dodecene-functionalized surfaces.[38] The high surface tension of the Hg drop likely inhibits the metal film interaction and subsequent displacement. It is unclear the origin of the widely disparate results for Al/OA reported here and Al/octadecene reported in ref 37. At a minimum, it indicates that the performance of directly attached films is highly variable.

Summary

To summarize, we have developed and used a novel pb-RAIRS technique to investigate the interaction between evaporative metals and molecular monolayers. Electrical device characterization was done to determine the relationship between the experimentally determined monolayer structure and molecular electronic device performance. The agreement between these two complementary in situ probes increases our confidence in the results and their interpretation. We observe surprisingly little interaction between evaporative Al and Au top-metal contacts on monolayers of OTS attached to silicon oxides. The monolayers are slightly degraded, and there is evidence of some metal interpenetration, but it appears that the metal principally remains on top of the films. Ti, however, strongly interacts with the molecular monolayer, but does not completely consume it. On the other hand, evaporative metals appear to completely

displace molecular monolayers directly attached to silicon via UV-assisted attachment of alcohols. This dramatic difference in monolayer stability illustrates that the substrate−monolayer interfacial chemistry can play a critical role in the interaction of organic monolayers and top metals.

Acknowledgment. We wish to thank S. Szeih for assistance in preparation of the OTS films, the NIST Microfabrication Facility and S. Hsu for use of their respective clean room facilities, and Oleg Kirillov for help with sample preparation.

Supporting Information Available: CV results for air plasma and UVO-treated SiO_2 films and a discussion of the modeling of the pb-RAIRS data. These materials are available free of charge via the Internet at http://pubs.acs.org.

References and Notes

(1) Schreiber, F. *Prog. Surf. Sci.* **2000**, *65*, 151−256.
(2) Boulas, C.; Davidovits, J. V.; Rondelez, F.; Vuillaume, D. *Phys. Rev. Lett.* **1996**, *76*, 4797−4800.
(3) Kagan, C. R.; Ratner, M. A. *MRS Bull.* **2004**, *29*, 376−381. Hersham M. C.; Reifenberger, R. G. *MRS Bull.* **2004**, *29*, 385−390. Ghosh, A.; Damle, P.; Datta, S.; Nitzan, A. *MRS Bull.* **2004**, *29*, 391−395. Kushmerick, J. G.; Allara, D. L.; Mallouk, T. E.; Mayer, T. S. *MRS Bull.* **2004**, *29*, 396−402.
(4) Stewart, D. R.; Ohlberg, D. A. A.; Beck, P. A.; Chen, Y.; Williams, R. S.; Jeppesen, J. O.; Nielson, K. A.; Stoddart, J. F. *Nano Lett.* **2004**, *4*, 133−136.
(5) Richter, C. A.; Stewart, D. R.; Ohlberg, D. A. A.; Chen, Y.; Williams, R. S. *Appl. Phys. A* **2005**, *80*, 1355−1362.
(6) Jun, Y.; Zhu, X.-Y. *J. Am. Chem. Soc.* **2004**, *126*, 13224−13225.
(7) Bierhals, A.; Aberle, A. G.; Hezel, R. *J. Appl. Phys.* **1998**, *83*, 1371−1378.
(8) Brixner, B. *J. Opt. Soc. Am.* **1965**, *55*, 1205.
(9) Richter, C. A.; Hacker, C. A.; Richter, L. J.; Vogel, E. M. *Solid-State Electron.* **2004**, *48*, 1747−1752.
(10) Hacker, C. A.; Anderson, K. A.; Richter, L. J.; Richter, C. A. *Langmuir* **2005**, *21*, 882−889.
(11) Film thickness was determined from SE and a three-phase (air, OA, Si) model, assuming an index of 1.5 for the alkoxy monolayer.
(12) Thicknesses are nominal, based on a quartz crystal micro balance monitor.
(13) Ti only capacitors (∼80 nm thick Ti) were fabricated for electrical characterization. Because of the poor IR reflectivity of Ti, blanket films consisting of a Ti:Au (9 nm/200 nm) stack were used for the pb-RAIRS measurements. Electrical measurements on Ti:Au capacitors were problematic due to poor registry of the two metal depositions due to the use of a shadow mask.
(14) Harder, P.; Bierbaum, K.; Woell, Ch.; Grunze, M.; Heid, S.; Effenberger, F. *Langmuir* **1997**, *13*, 445−454.
(15) *Practical Fourier Transform Infrared Spectroscopy*; Ferraro, J. R., Krishnan, K. Eds.; Academic: San Diego, 1990; Chapter 6.
(16) MacPhail, R. A.; Strauss, H. L.; Snyder, R. G.; Elliger, C. A. *J. Phys. Chem.* **1984**, *88*, 334−341.
(17) Snyder, R. G.; Strauss, H. L.; Elliger, C. A. *J. Phys. Chem.* **1982**, *86*, 5145−5150.
(18) McGovern, W. R.; Anariba, F.; McCreery, R. L. *J. Electrochem. Soc.* **2005**, *152* (5), E176−E183.
(19) Hacker, C. A.; Richter, C. A.; Richter, L. J. *AIP Conference Proceedings* **2005**, (788), 610−614.
(20) Trasferetti, B. C.; Davanzo, C. U.; Da Cruz, N. C.; de Moraes, M. A. B. *Appl. Spec.* **2000**, *54*, 687−691.
(21) Yamamoto, M.; Sakurai, Y.; Hosoi, Y.; Ishii, H.; Ito, E.; Kajikawa, K.; Ouchi, Y.; Seki, K. *Surf. Sci.* **1999**, *427*, 388−392, and references therein.
(22) Konstadinidis, K.; Zhanf, P.; Opila, R. L.; Allara, D. L. *Surf. Sci.* **1995**, *338*, 300−312.
(23) de Boer, B.; Frank, M. M.; Chabal, Y. J.; Jiang, W.; Garfunkel, E.; Bao, Z. *Langmuir* **2004**, *20*, 1539−1542.
(24) The input face oxide film was not included as it is removed by the reference spectrum.
(25) *Handbook of Optical Constants of Solids II*; Palik, E. D., Ed.; Academic Press: 1991.
(26) Parikh, A. N.; Allara, D. L.; Azouz, I. B.; Rondelez, F. *J. Phys. Chem.* **1994**, *98*, 7577−7590.
(27) The experimental measurement uncertainty for an IV measurement for any given capacitor structure is very small (less than the width of the line in Figures 2 and 3). The device−device variability is moderate (disregarding the occasional device outliers), and the IV curves shown are representative of the majority of the measured devices. For Au−metal devices (where we have the most measurements and fabrication runs), the fabrication-run−fabrication-run variability is comparable to the dot−dot variability within a given fabrication run.
(28) Walker, A. V.; Tighe, T. B.; Cabarcos, O. M.; Reinard, M. D.; Haynie, B. C.; Uppolo, S.; Winograd, N.; Allara, D. L. *J. Am. Chem. Soc.* **2004**, *126*, 3954−3963.
(29) Hooper, A.; Fisher, G. L.; Konstadinidis, K.; Jung, D.; Nguyen, H.; Opila, R.; Collins, R. W.; Winograd, N.; Allara, D. L. *J. Am. Chem. Soc.* **1999**, *121*, 8052−8064.
(30) Buriak, J. M. *Chem. Rev.* **2002**, *102*, 1272−1308.
(31) Haber, J. A.; Lewis, N. S. *J. Phys. Chem. B* **2002**, *106*, 3639−3656.
(32) *Organosilicon Compounds*; Bazant, V., Chvalovsky, V., Rathousky, J., Eds.; Academic Press: New York, 1965.
(33) Kim, N. Y.; Labinis, P. E. *J. Am. Chem. Soc.* **1997**, *119*, 2297.
(34) Boukherroub, R.; Morin, S.; Sharpe, P.; Wayner, D. D. M.; Allongue, P. *Langmuir* **2000**, *16*, 7429.
(35) Herdt, G. C.; Jung, D. R.; Czanderna, A. W. *J. Adhes.* **1997**, *60*, 197−222.
(36) Walker, A. V.; Tighe, T. B.; Haynie, B. C.; Upili, S.; Winograd, N.; Allara, D. L. *J. Phys. Chem. B* **2005**, *109*, 11263−11272.
(37) Kar, S.; Miramond, C.; Vuillaume, V. *Appl. Phys. Lett.* **2001**, *78*, 1288−1291.
(38) Liu, Y.-J.; Yu, H.-Z. *ChemPhysChem* **2003**, *4*, 335−342.